

Properties of the Poynting vector for invariant beams: negative propagation in Weber beams

Irving Rondón and F. Soto-Eguibar,
Instituto Nacional de Astrofísica Óptica y Electrónica,
Puebla, C.P. 72840 México.

August 11, 2020

Abstract

Negative propagation is an uncommon response produced by the local sign change in Poynting vector components. We present a general Poynting vector expression for all invariant beams with cylindrical symmetry using scalar potentials in order to evaluate the possibility of negative propagation. We analyze the plausibility of negative propagation being independent of mode mixing; we study Weber beams as a particular case. The study of this negative effect allow us to advance in the field of micro manipulation and understanding of optical forces. Applications of these beams are discussed.

1 Introduction

Propagation invariant beams, also known as “non-diffracting beams”, propagate indefinitely without changing their transverse intensity distribution. These invariant beams retain some of their peculiar characteristics: the basic transverse shape of the field is preserved along their propagation. Some interesting properties are absence of diffraction, self-reconstruction, highly focused field distributions and angular momentum transfer. Novel problems have been addressed and their applications have been recently reported in [1]. These optical fields are the well known plane waves, Bessel beams [2], Mathieu beams [3] and Weber beams [4]. The study of these fields cover different areas, such as quantum optics [5, 6, 7, 8, 9], nonlinear optics [10], optical communications [11], mechanical transfer of orbital angular momentum to trapped particles in optical tweezers [12], trapping forces [13], acoustic optics [14], scattering problems using partial waves series in the far field approximation [15, 16, 17, 18], and angular momentum [19], among others.

In order to obtain the maximum possible information from these fields, it is very important to have a deeper insight of their physical properties. One of the key electromagnetic quantities is Poynting vector. The Bessel beams case has been successfully studied, both experimentally [20] and theoretically [21, 22]. A complete study has also been done for Airy beams, first reported in [23] where the Poynting vector’s evolution and angular momentum are analyzed. The authors in [24] have recently shown that Bessel beams possess negative values in the longitudinal and azimuthal components of the Poynting vector, depending on the phase detuning between the complex amplitudes c_{TE} and c_{TM} of the transversal electric part (TE) and the transversal magnetic part (TM) of the beam. It should be noted that the Poynting vector’s negative sign was investigated earlier for interference of four linearly polarized plane waves in [25], but the author concluded that this fact does not have a realistic physical interpretation. Another interesting case was reported for X-Waves, where the propagation direction of their negative Poynting vector could be locally changed using carefully chosen complex amplitudes [26]. Nonetheless, the negative Poynting vector behavior presented in the Bessel beams and in the X-Waves, mentioned above, has opened a discussion related to tractor beams generation, and other interesting applications, such as the forces that can be locally oriented in a direction opposite of the propagation wave vector [27]. Examples of this last type of forces are: optical pulling force [28], negative effects in metamaterials [29], the optical forces process induced by nonparaxial gradient-less beams [30], the origin of universal optical traction [31], the application of negative longitudinal optical force under the illumination of Bessel beam of arbitrary order, and polarization [32]. On the other hand, in [33], the authors found a negative propagation effect in the Airy nonparaxial beams for which a complex superposition of Transverse Electric (TE) and Transverse Magnetic (TM) modes is not mandatory. Otherwise, for Bessel beams and for X-Waves beams, the local negativeness depends on the mixed modes TE/TM superposition.

Despite the considerable research on optical invariant beams, a general description of the Poynting vector in nonparaxial beams has not been presented, and the applications previously mentioned still remain unexplored for the Weber beam case. A need to understand their physical properties is necessary due to recent interesting works that have been reported

using invariant beams, such as optical surfaces waves [34, 35], application in laser beam shaping [36], meta-surfaces [37], optical forces [38], scattering [39], among others. Many of these works, however, are based on plane waves and attempts with Bessel beams. To the best of our knowledge, very little attention has been reported for the Weber beams Poynting vector, considering any invariant beam and using the scalar potential description. We propose an alternative approach to achieve a description of the local negative properties for the Poynting vector. We show that mixed electromagnetic modes TE/TM are not a compulsory condition to display negative propagation for invariant beams. The transverse structure of the Weber beams can also be applied in “tractor beams” [40]. Since the experiments carried out for the “Bessel-tractor” case only works in short distances [41], other applications such as optical and scattering forces can be explored [42]. This article is structured as follows: in Section 2, we develop the theoretical framework based on the scalar potential approach; in Section 3, we present the general Poynting vector for all family invariant beams and we give some examples, as the plane wave and Bessel beam; in Section 4, we consider the case of Weber beams; and finally, in Section 5, we present our conclusions.

2 The scalar potential as a general solution for Maxwell equations

It is well known that Maxwell’s equations can be written using a general vector basis in a boundary value problem dealing with linear, isotropic, homogeneous, and time-invariant media, where these vector eigenfunctions are derived from the complete set of separable solutions of the scalar Helmholtz equation [43]. The method of coupling a pair of scalar functions with adequate boundary conditions for the electric and magnetic fields, was originally proposed to find solutions to the problem of scattering of electromagnetic waves from a dielectric sphere. In [44], and references therein, the reader can find an interesting review of this topic and practical examples are given in [45].

In this work, we follow the formalism proposed by Stratton in [46] to study the properties of vector beams in cylindrical symmetry electromagnetic fields. In this formalism, the electromagnetic fields are written as

$$\vec{E} = c_{TE}\vec{M}(\vec{r}) + c_{TM}\vec{N}(\vec{r}), \quad (1a)$$

$$\vec{H} = -i\sqrt{\frac{\varepsilon}{\mu}} \left[c_{TE}\vec{N}(\vec{r}) + c_{TM}\vec{M}(\vec{r}) \right], \quad (1b)$$

being $\vec{M}(\vec{r})$ and $\vec{N}(\vec{r})$ vector fields defined by

$$\vec{M}(\vec{r}) = \nabla \times [\hat{a}\psi(\vec{r})], \quad (2)$$

and

$$\vec{N}(\vec{r}) = \frac{1}{k}\nabla \times \vec{M}(\vec{r}), \quad (3)$$

where ψ is a scalar field, \hat{a} is an arbitrary unit vector that determines the direction of propagation (which we will choose as the Z axes, so $\hat{a} = \hat{e}_3$), k is the magnitude of the wave vector, ε is the electric permittivity, μ is the magnetic permeability, and c_{TE} and c_{TM} are two arbitrary complex numbers [47].

It is straightforward to verify that if the scalar field $\psi(\vec{r})$ satisfies the scalar Helmholtz equation,

$$\nabla^2\psi + k^2\psi = 0, \quad (4)$$

then the fields (1a) and (1b) satisfy the Maxwell equations; so, the scalar field $\psi(\vec{r})$ will be named scalar potential. Note that the vector fields, \vec{M} and \vec{N} , are orthogonal between them, that is $\vec{M} \cdot \vec{N} = 0$, and solenoidal, i.e. $\nabla \cdot \vec{M} = 0$ and $\nabla \cdot \vec{N} = 0$.

Though the homogeneous (source-free) Helmholtz equation can be separated in eleven coordinate systems, we require separability into transverse and longitudinal parts, and that is possible only in Cartesian, cylindrical, parabolic cylindrical and elliptical cylindrical coordinates [43]. The spatial evolution of the scalar potential ψ can then be described by the transverse and the longitudinal parts. The transverse part $\varphi(u_1, u_2)$ will depend only on the transverse coordinates, u_1, u_2 , and the longitudinal part $Z(z)$ will depend on the longitudinal coordinate z (as we choose $\hat{a} = \hat{e}_3$). Therefore

$$\psi(u, v, z) = \varphi(u_1, u_2)Z(z). \quad (5)$$

After substituting (5) in the Helmholtz equation, we easily obtain that $\varphi(u_1, u_2)$ satisfies the two dimensional transverse Helmholtz equation

$$\nabla_T^2\varphi + k_T^2\varphi = 0, \quad (6)$$

where ∇_T^2 is the Laplacian transversal operator which has a specific form in each coordinate system, and the longitudinal part is $Z(z) = e^{ik_z z}$ with the dispersion relation $k^2 = k_T^2 + k_z^2$. As previously stated, the two dimensional transverse

Helmholtz equation (6) can be separated in Cartesian, cylindrical, parabolic cylindrical and elliptical cylindrical coordinates [43], and that gives origin to the plane waves, Bessel beams, Weber beams and Mathieu beams, respectively. Then we can write

$$\vec{M} = -e^{ik_z z} \nabla_T^\perp \varphi, \quad (7)$$

where

$$\nabla_T^\perp = -\hat{e}_1 \frac{1}{h_2} \frac{\partial}{\partial u_2} + \hat{e}_2 \frac{1}{h_1} \frac{\partial}{\partial u_1}, \quad (8)$$

\hat{e}_1 and \hat{e}_2 are the base unit vectors corresponding to the transversal direction, and h_1 and h_2 are the corresponding scale factors. We note that in the four coordinate systems we are studying, the scale factor h_3 is equal to 1. It is also very easy to see that

$$\vec{N} = \frac{e^{ik_z z}}{k} (ik_z \nabla_T + \hat{e}_3 k_T^2) \varphi, \quad (9)$$

where

$$\nabla_T = \hat{e}_1 \frac{1}{h_1} \frac{\partial}{\partial u_1} + \hat{e}_2 \frac{1}{h_2} \frac{\partial}{\partial u_2}. \quad (10)$$

It is important to note that the scalar potential can be used to analyze any invariant beam. In the case of Bessel beams, this formalism was thoroughly used for analyzing them theoretically in [48, 49, 50], and in [51] to study experimentally its TE and TM modes.

In the particular case of Weber beams, its transversal structure is naturally described in terms of parabolic coordinates u and v , related to the Cartesian through the following transformation

$$x + iy = \frac{1}{2}(u + iv)^2, \quad z = z, \quad (11)$$

where x , y and z are the corresponding Cartesian coordinates with $u \in (-\infty, +\infty)$ and $v \in [0, +\infty)$. The scaling factors for the parabolic coordinate system are given by

$$h_1 = h_2 = \sqrt{u^2 + v^2}. \quad (12)$$

3 A general expression for the transversal and longitudinal beam propagation modes

The Poynting vector represents the directional power flux per unit area of an electromagnetic field. For harmonic electromagnetic fields, its time average is given by [52]

$$\langle \vec{S} \rangle = \frac{1}{2} \text{Re} \left(\vec{E} \times \vec{H}^* \right). \quad (13)$$

Writing the electromagnetic fields, (1a) and (1b), in terms of the scalar potential φ , we can obtain the time averaged Poynting vector for any invariant beams as a sum of a transversal and a longitudinal part,

$$\langle \vec{S} \rangle = \langle \vec{S} \rangle_T + \langle \vec{S} \rangle_z, \quad (14)$$

where the transversal Poynting vector is

$$\begin{aligned} \langle \vec{S} \rangle_T &= \frac{k_T^2}{2k^2} \sqrt{\frac{\varepsilon}{\mu}} \times \\ &\text{Re} \left[-i \left(|c_{\text{TE}}|^2 \varphi^* \nabla_T \varphi - |c_{\text{TM}}|^2 \varphi \nabla_T \varphi^* \right) k + k_z c_{\text{TE}}^* c_{\text{TM}} \hat{e}_3 \times \nabla_T (\varphi^* \varphi) \right], \end{aligned} \quad (15)$$

and the longitudinal Poynting vector is

$$\begin{aligned} \langle \vec{S} \rangle_z &= \frac{\hat{e}_3}{2k^2} \sqrt{\frac{\varepsilon}{\mu}} \text{Re} \left[\left(|c_{\text{TE}}|^2 + |c_{\text{TM}}|^2 \right) k k_z (\nabla_T \varphi \cdot \nabla_T \varphi^*) \right. \\ &\quad \left. + i (c_{\text{TE}} c_{\text{TM}}^* k^2 + c_{\text{TE}}^* c_{\text{TM}} k_z^2) (\nabla_T \varphi^* \times \nabla_T \varphi) \cdot \hat{e}_3 \right] \end{aligned} \quad (16)$$

The expressions (15) and (16) give all the information about the Poynting vector for any invariant beam, and they provide information related with a particular mode TE or TM and the possible mixed modes. These expressions possess an interference part which generally is not zero. Note that these results show that the time averaged Poynting vector is independent of the z coordinate, as expected. In order to emphasize the non-diffractive character of these beams, it was proven that the divergence of the transversal part of the time averaged Poynting vector is zero [53]. All the previous argumentations show that when mixed modes are present, the acquisition of electromagnetic properties is straightforward using the scalar approach [54].

The next step is to generalize the procedure proposed in [24], for Bessel beams, to any invariant beam. The substitution of $c_{\text{TE}} = |a_1|e^{i\phi_1}$ and $c_{\text{TM}} = |a_2|e^{i\phi_2}$ in the equations (15) and (16) shows directly that any invariant beam has negative behavior due to mixed modes; mathematically, a periodic function cosine or sine, with certain phase differences, can be presented, as was reported for Bessel beams [24]. However, recently it has been stated in [33] that the negative behavior can be found independently of the mode interference. In order to validate the possibility of negative local Poynting vector behavior, let us use equations (15) and (16) in the mixed components, in the following examples.

In the case of a plane wave, where the solution of the transversal Helmholtz equation is $\varphi(x, y) = \exp[i(k_x x + k_y y)]$, it is very easy to show that $\text{Re}[c_{\text{TE}}^* c_{\text{TM}} \hat{e}_3 \times \nabla_T(\varphi^* \varphi)] = 0$, and that $\text{Re}[i(c_{\text{TE}} c_{\text{TM}}^* k^2 + c_{\text{TE}}^* c_{\text{TM}} k_z^2)(\nabla_T \varphi^* \times \nabla_T \varphi)] = 0$; therefore, the interference term is zero. However, negative propagation can be found using several plane waves; indeed, two plane waves are sufficient [25], without mixed modes.

For the Bessel beams, it is very well known that the transversal field is $\varphi(r, \theta) = J_m(k_T r) \exp(im\theta)$; and in this case we have that $\text{Re}[c_{\text{TE}}^* c_{\text{TM}} \hat{e}_3 \times \nabla_T(\varphi^* \varphi)]$ and $\text{Re}[i(c_{\text{TE}} c_{\text{TM}}^* k^2 + c_{\text{TE}}^* c_{\text{TM}} k_z^2)(\nabla_T \varphi^* \times \nabla_T \varphi)]$ are both different from zero, which implies negative propagation in the azimuthal and longitudinal components [24]. In the next section, the hitherto unreported negative behavior of the Poynting vector in the case of Weber beams will be considered.

4 The Poynting vector of Weber beams

The existence of parabolic optical fields has been demonstrated theoretically and experimentally for the first time by Bandres et. al. [4, 5]. At the present time, several interesting investigations have been done, such as quantum experimental observation of the scattering of free falling dilute thermal clouds of ^{38}Rb atoms [55] and the manipulation of microscopic particles driven by parabolic beams [56]. The physical properties of Weber beams have been recently studied, such as accelerating beams [57, 58]. Their implications for many linear wave systems in nature and its applications in diverse scenarios have been evaluated [59].

The scalar potential of the Weber beams can be expressed as a product of parabolic functions; for the even Weber beams,

$$\varphi_e(u, v) = \frac{1}{\pi\sqrt{2}} |\Gamma_1|^2 U_e(u, a) U_e(v, -a), \quad (17)$$

and for the odd Weber beams,

$$\varphi_o(u, v) = \frac{1}{\pi\sqrt{2}} |\Gamma_3|^2 U_o(u, a) U_o(v, -a), \quad (18)$$

where the subscripts e and o stand for even and odd, respectively; a is essentially the separation constant, that we will consider real, $\Gamma_1 = \Gamma(\frac{1}{4} + i\frac{a}{2})$ and $\Gamma_3 = \Gamma(\frac{3}{4} + i\frac{a}{2})$ are normalization constants, being $\Gamma(\zeta)$ the gamma function, and the U functions are given by

$$U_e(u, a) = \exp\left(-i\frac{1}{2}k_T u^2\right) {}_1F_1\left(\frac{1}{4} - i\frac{a}{2}, \frac{1}{2}, ik_T u^2\right), \quad (19)$$

and by

$$U_o(u, a) = u \exp\left(-i\frac{1}{2}k_T u^2\right) {}_1F_1\left(\frac{3}{4} - i\frac{a}{2}, \frac{3}{2}, ik_T u^2\right), \quad (20)$$

with ${}_1F_1(\alpha, \beta, \zeta)$ the confluent hypergeometric function. In Figures 1 and 2, the absolute value of the Weber beams, even (17) and odd (18), are shown for $a = 0$ and $k_T = 1 \text{ m}^{-1}$, in terms of the Cartesian coordinates. If we substitute equations (17) to (20) in (15) and (16), we obtain, after a very long calculation, the general Poynting vector for the even and odd Weber beams; in this Poynting vector the transversal and longitudinal interference terms are not zero, thus there will be negative propagation. To simplify the analysis, we will consider here only the case $a = 0$; we have chosen this value for the sake of simplicity and because these particular Weber beams have been used to study the scattering by a rigid sphere centered along the propagation axis [18], to analyze the transversal behavior and for inspect some features of their

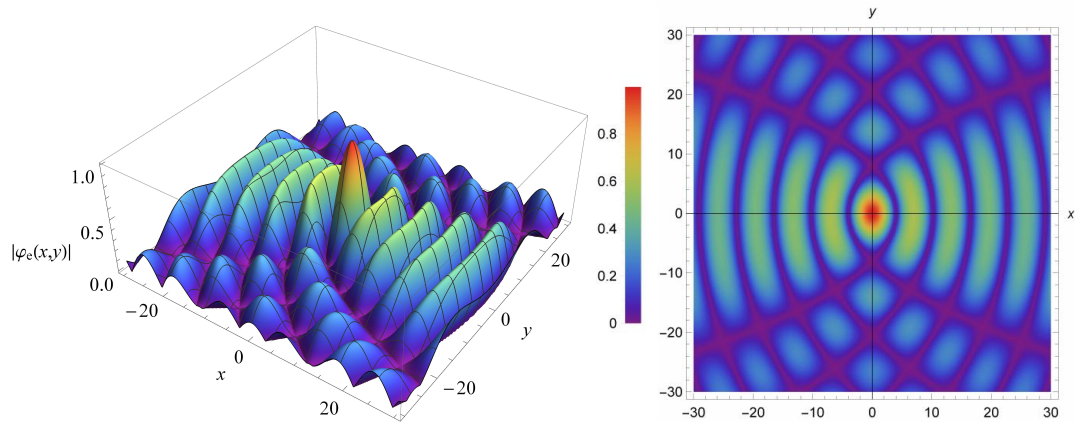


Figure 1: Absolute value of the even Weber beams (17) for $a = 0$ and $k_T = 1 \text{ m}^{-1}$. Colors represent the absolute value of the even Weber beams according to the bar shown.

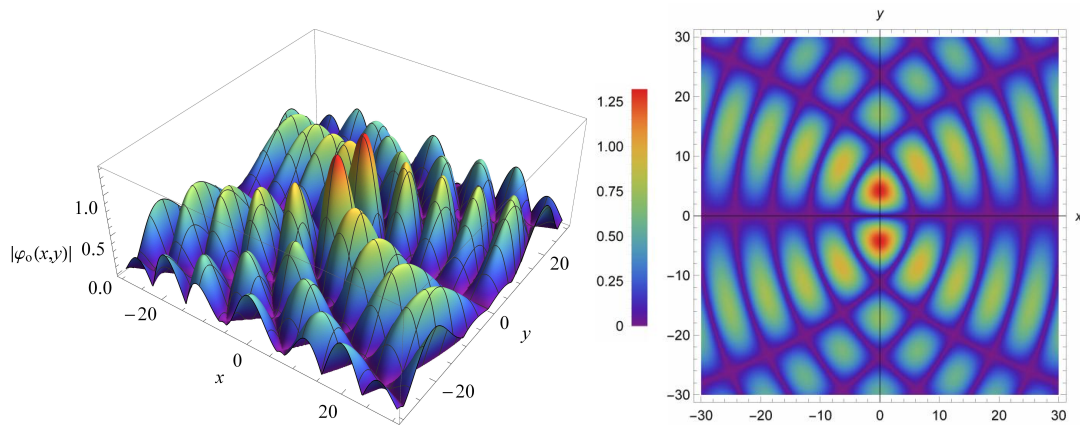


Figure 2: Absolute value of the odd Weber beams (18) for $a = 0$ and $k_T = 1 \text{ m}^{-1}$. The colors represent the absolute value of the odd Weber beams according to the bar shown.

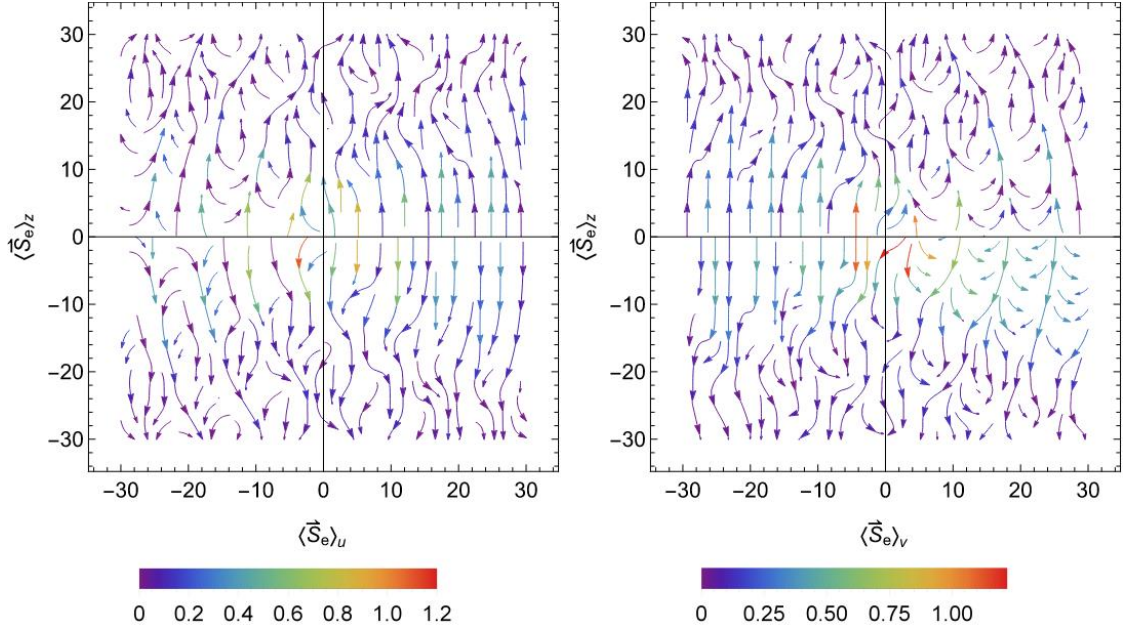


Figure 3: Streamlines of the two dimensional vector fields $(\langle \vec{S}_e \rangle_u, \langle \vec{S}_e \rangle_z)$ and $(\langle \vec{S}_e \rangle_v, \langle \vec{S}_e \rangle_z)$, for $a = 0$, $k_T = 1 \text{ m}^{-1}$ and $\phi_1 = \phi_2$. The plots streamlines show the local direction of the vector field at each point and the arrows are colored according to the magnitude of the field, as presented in the bars below.

normalization [60]. Thus, when $a = 0$, we obtain for the even Weber beams,

$$\begin{aligned} \langle \vec{S}_e \rangle_u &= \frac{k_T^4}{4k^2} \sqrt{\frac{\varepsilon}{\mu}} \frac{k_z v^2}{\sqrt{u^2 + v^2}} \Gamma^4 \left(\frac{3}{4} \right) |u| J_{-\frac{1}{4}}^2 \left(\frac{k_T u^2}{2} \right) J_{-\frac{1}{4}} \left(\frac{k_T v^2}{2} \right) \times \\ &\quad J_{\frac{3}{4}} \left(\frac{k_T v^2}{2} \right) \cos(\phi_1 - \phi_2), \end{aligned} \quad (21a)$$

$$\begin{aligned} \langle \vec{S}_e \rangle_v &= -\frac{k_T^4}{4k^2} \sqrt{\frac{\varepsilon}{\mu}} \frac{k_z u v}{\sqrt{u^2 + v^2}} \Gamma^4 \left(\frac{3}{4} \right) |u| J_{-\frac{1}{4}} \left(\frac{k_T u^2}{2} \right) J_{\frac{3}{4}} \left(\frac{k_T u^2}{2} \right) \times \\ &\quad J_{-\frac{1}{4}}^2 \left(\frac{k_T v^2}{2} \right) \cos(\phi_1 - \phi_2), \end{aligned} \quad (21b)$$

$$\begin{aligned} \langle \vec{S}_e \rangle_z &= \frac{k_T^3 k_z}{4k} \sqrt{\frac{\varepsilon}{\mu}} \frac{v |u|}{u^2 + v^2} \Gamma^4 \left(\frac{3}{4} \right) \times \\ &\quad \left[v^2 J_{-\frac{1}{4}}^2 \left(\frac{k_T u^2}{2} \right) J_{\frac{3}{4}}^2 \left(\frac{k_T v^2}{2} \right) + u^2 J_{\frac{3}{4}}^2 \left(\frac{k_T u^2}{2} \right) J_{-\frac{1}{4}}^2 \left(\frac{k_T v^2}{2} \right) \right]. \end{aligned} \quad (21c)$$

We can observe the presence of spatial variations for $\langle \vec{S}_e \rangle_u$ and $\langle \vec{S}_e \rangle_v$ due to the phase difference between modes, as was reported for the Bessel beam case in [24]. However, even when the phase difference is zero, $\phi_1 = \phi_2$, we have negative values for all three components of the Poynting vector. The Poynting vector of the Weber beams has a very complex vector structure. In order to give an idea of this complex compartment, we show in Figure (3) the streamlines of the two dimensional vector fields $(\langle \vec{S}_e \rangle_u, \langle \vec{S}_e \rangle_z)$ and $(\langle \vec{S}_e \rangle_v, \langle \vec{S}_e \rangle_z)$, obtained as combinations of the two transverse components with the longitudinal component; the plots streamlines show the local direction of the vector field at each point and the arrows are colored according to the magnitude of the field, as presented in the bars below each one. The behavior of the trajectories and their relation with the parameters can be explained from the point of view of dynamical systems [61], but that goes beyond the scope of this work. As we already mention, these results show that for the longitudinal component vector, given by (21c), there is not presence of mixed modes, which was the hypothesis for negative propagation in [24]. The negative propagation for the longitudinal component is shown in Figure (4). Following the same procedure,

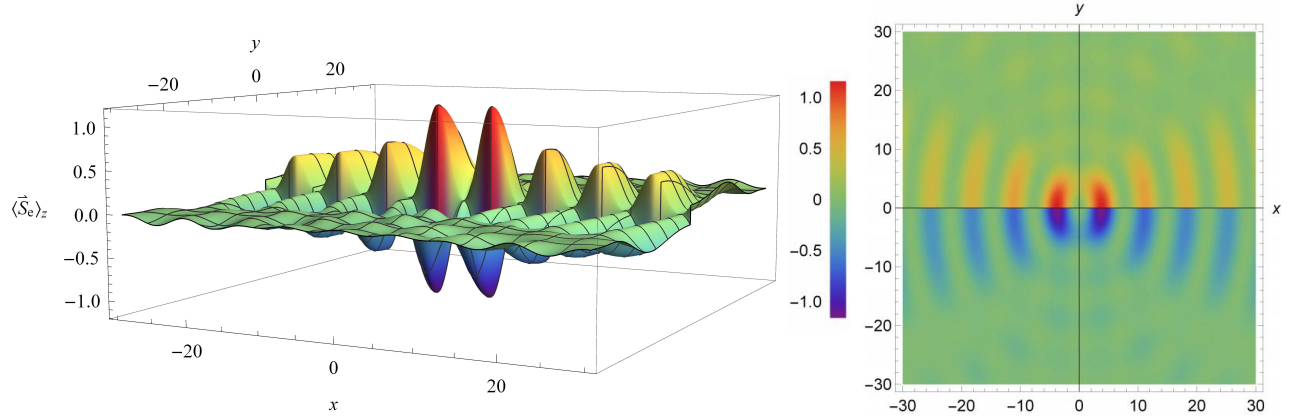


Figure 4: Tridimensional behavior of the longitudinal component of the Poynting vector, $\langle \vec{S}_e \rangle_z$, for even Weber beams ($a = 0$, $k_T = 1 \text{ m}^{-1}$). The colors represent the values of the z -component of the Poynting vector, according to the bar shown.

we found for the odd case,

$$\begin{aligned} \langle \vec{S}_o \rangle_u &= -\frac{k_T^2 k_z |v|}{k^2 |u|} \sqrt{\frac{\varepsilon}{\mu}} \frac{u^2 v}{\sqrt{u^2 + v^2}} \Gamma\left(\frac{1}{4}\right) \Gamma\left(\frac{5}{4}\right)^3 J_{\frac{1}{4}}^2\left(\frac{k_T u^2}{2}\right) \times \\ &J_{-\frac{3}{4}}\left(\frac{k_T v^2}{2}\right) J_{\frac{1}{4}}\left(\frac{k_T v^2}{2}\right) \cos(\phi_1 - \phi_2) \end{aligned} \quad (22a)$$

$$\begin{aligned} \langle \vec{S}_o \rangle_v &= \frac{k_T^2 k_z}{k^2 |u|} \sqrt{\frac{\varepsilon}{\mu}} \frac{u^3 v}{\sqrt{u^2 + v^2}} \Gamma\left(\frac{1}{4}\right) \Gamma\left(\frac{5}{4}\right)^3 J_{-\frac{3}{4}}\left(\frac{k_T u^2}{2}\right) \times \\ &J_{\frac{1}{4}}\left(\frac{k_T u^2}{2}\right) J_{\frac{1}{4}}^2\left(\frac{k_T v^2}{2}\right) \cos(\phi_1 - \phi_2), \end{aligned} \quad (22b)$$

$$\begin{aligned} \langle \vec{S}_o \rangle_z &= \frac{4k_T k_z}{k} \sqrt{\frac{\varepsilon}{\mu}} \frac{v |u|}{u^2 + v^2} \Gamma^4\left(\frac{5}{4}\right) \times \\ &\left[u^2 J_{-\frac{3}{4}}^2\left(\frac{k_T u^2}{2}\right) J_{\frac{1}{4}}^2\left(\frac{k_T v^2}{2}\right) + v^2 J_{\frac{1}{4}}^2\left(\frac{k_T u^2}{2}\right) J_{-\frac{3}{4}}^2\left(\frac{k_T v^2}{2}\right) \right]. \end{aligned} \quad (22c)$$

As in the even case, the negative propagation appears even if there are no mixed modes. As expected, the behavior of the Poynting vector in this case is as complex as in the even case, and to visualize it we present Figure (5) where the streamlines of the two dimensional vector fields $(\langle \vec{S}_o \rangle_u, \langle \vec{S}_o \rangle_z)$ and $(\langle \vec{S}_o \rangle_v, \langle \vec{S}_o \rangle_z)$, obtained as combinations of the two transverse components with the longitudinal component, are plotted; the plots streamlines show the local direction of the vector field at each point and the arrows are colored according to the magnitude of the field, as presented in the bars below each one. The negative energy propagation in the longitudinal component $\langle \vec{S}_o \rangle_z$ of the odd Weber beams is shown in Figure (6).

5 Conclusions

We have obtained a general expression for the Poynting vector using a scalar approach, and we have shown its potential to study the energy negative behavior for any invariant beam with cylindrical symmetry. The expression obtained for the Poynting vector brings to the fact that all nonparaxial beams have the possibility of negative local change in the Poynting vector, independently of the presence of mixed modes. In the case of Weber beams, we have shown explicitly that negative propagation exists. In the longitudinal direction, $S_z < 0$ independently of the difference between c_{TE} and c_{TM} for $a = 0$. The presence of negative propagation regions in Weber beams can provide new applications, such as trapping, because the variation of the Poynting vector sign can create multiple traps and bounding particles. Recently the authors in [62] have reported the use of optical engineering and light-matter interaction for emerging optical manipulation and its applications, but the Weber beam case still needs to be explored.

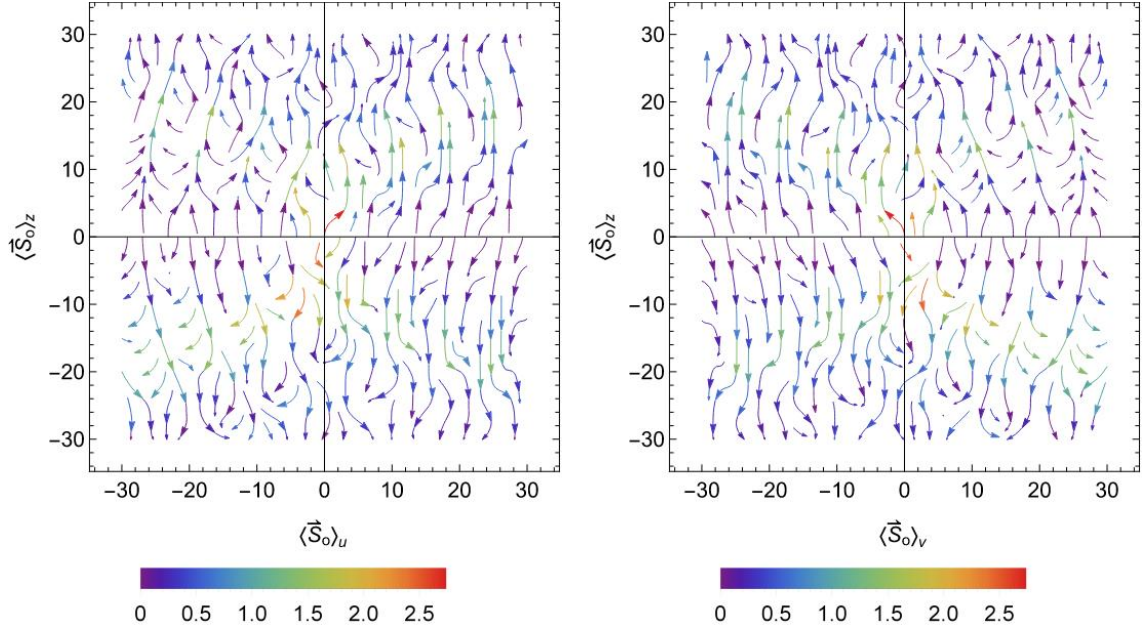


Figure 5: Streamlines of the two dimensional vector fields $(\langle \vec{S}_o \rangle_u, \langle \vec{S}_o \rangle_z)$ and $(\langle \vec{S}_o \rangle_v, \langle \vec{S}_o \rangle_z)$, for $a = 0$, $k_T = 1 \text{ m}^{-1}$ and $\phi_1 = \phi_2$. The plots streamlines show the local direction of the vector field at each point and the arrows are colored according to the magnitude of the field, as presented in the bars below.

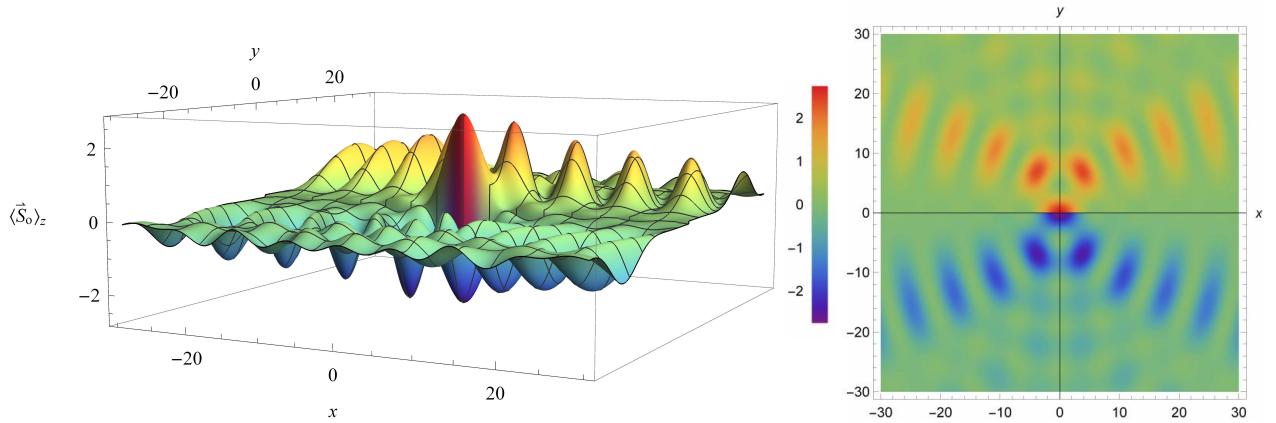


Figure 6: Tridimensional behavior of the longitudinal component of the Poynting vector, $\langle \vec{S}_o \rangle_z$, for odd Weber beams ($a = 0$, $k_T = 1 \text{ m}^{-1}$). The colors represent the values of the z -component of the Poynting vector, according to the bar shown.

6 Acknowledgments

I. Rondon-Ojeda thanks and acknowledges the support given by SEP-PRODEP postdoctoral program UMSNH-CA-221 at Laboratory of Optical Sensors. The authors also want to thank Douglas David Crockett, Volunteer of Peace Corps Response at INAOE, for reading and improve the manuscript . We also want to thank the unknown reviewers and the editor of this journal for several valuable corrections and comments.

References

- [1] H.E Hernández-Figueroa, M. Zamboni-Rached and E. Recami , *Non-diffracting Waves* John Wiley & Sons, (2013).
- [2] J. Durnin, “Exact solutions for nondiffracting beams. I. The scalar theory,” *J. Opt. Soc. Am. A*, 4 (1987) 4, 651-654,
- [3] J.C Gutiérrez-Vega, M.D Iturbe-Castillo and S. Chávez-Cerda, “Alternative formulation for invariant optical fields: Mathieu beams,” *Opt. Letters*, 25 (2000) 20, 1493–1495.
- [4] M.A. Bandres, J.C. Gutiérrez-Vega and S. Chávez-Cerda, “Parabolic nondiffracting optical wave fields,” *Opt. Letters*, 29 (2004) 1, 44–46.
- [5] C. López-Mariscal, M. A. Bandres, S. Chávez-Cerda, and J. C. Gutiérrez-Vega, “Observation of Parabolic nondiffracting optical fields”, *Optics Express*, 13(7) (2005) 2364.
- [6] Jáuregui R. and Hacyan S., “Quantum-mechanical properties of Bessel beams,” *Phys. Rev. A* 71 (2005) 033411.
- [7] B.M. Rodríguez-Lara and R. Jáuregui, “Dynamical constants for electromagnetic fields with elliptic-cylindrical symmetry,” *Phys. Rev. A* 78 (2008) 033813.
- [8] B.M. Rodríguez-Lara and R. Jáuregui , “Dynamical constants of structured photons with parabolic-cylindrical symmetry,” *Phys. Rev. A* 79 (2009) 055806.
- [9] B.M. Rodríguez-Lara and R. Jáuregui, “Single structured light beam as an atomic cloud splitter,” *Phys. Rev. A* 80 (2009) 011813R.
- [10] T. Wulle and S. Herminghaus, “Nonlinear optics of Bessel beams,” *Phys. Rev. Lett.* 71 (1993) 209, 1401–1404.
- [11] A.E. Willner et al, “Optical communications using orbital angular momentum beams,” *Adv. Opt. Photon*, 7 (2015) 1, 66–106.
- [12] K. Volke-Sepulveda, et al “Orbital angular momentum of a high-order Bessel light beam,” *J. Opt. B: Quantum Semiclass. Opt.* 4 (2002) S82-S89.
- [13] L. A. Ambrosio and H.E. Hernández-Figueroa, “Integral localized approximation description of ordinary Bessel beams and application to optical trapping forces,” *Biomed. Opt. Express* 2 (2011) 7, 1893–1906.
- [14] L. Zhang and P.L. Marston, “Optical theorem for acoustic non-diffracting beams and application to radiation force and torque,” *Biomed. Opt. Express* 4 (2013) 9, 1610–1617.
- [15] P.L. Marston , “Scattering of a Bessel beam by a sphere,” *J. Acoust. Soc. Am.* 121 (2007) 2, 753–758.
- [16] P.L. Marston, “Scattering of a Bessel beam by a sphere II: Helicoidal case shell example,” *J. Acoust. Soc. Am.* 124 (2008) 5, 2905–2910.
- [17] A. Belafhal, A. Chafiq and Z. Hricha, “Scattering of Mathieu beams by a rigid sphere,” *Opt. Comm.* 284 (2011) 3030–3035.
- [18] A. Belafhal, L. Ez-Zariy, A. Chafiq and Z. Hricha Z., “Analysis of the scattering far field of a nondiffracting parabolic beam by a rigid sphere,” *Phys. and Chem. News*, 60 (2011) 15–21.
- [19] P. Brandao, “Nonparaxial TE and TM vector beams with well-defined orbital angular momentum,” *Opt. Letters*, 37 (2012) 5, 909–911.
- [20] Y. Lin, et al, “Experimental investigation of Bessel beam characteristics”, *Applied Opt.* 11 (1992) 15, 2708–2713.

- [21] I. Mokhun, et al, “Experimental analysis of the Poynting vector characteristics”, *Applied Opt.* 51 (2012) 10.
- [22] I. A. Litvin, “The behavior of the instantaneous Poynting vector of symmetrical laser beams,” *J. Opt. Soc. Am.* 29 (2012) 6, 901–907.
- [23] H.I. Sztul and R.R. Alfano, “The Poynting vector and angular momentum of Airy beams,” *Opt. Express* 16, (2008) 9411–9416.
- [24] A.V. Novitsky, and D. V. Novitsky, “Negative propagation of vector Bessel beams”, *J. Opt. Soc. Am. A* 24 (2007) 9.
- [25] B.Z. Katsenelenbaum, “What is the direction of the Poynting vector?”, *Journal of Communication and Electronics*, 42 (1997) 2, 119.
- [26] M. A. Salem and H. Bagci, “Energy flow characteristics of vector X-Waves”, *Opt. Express* 19 (2011) 8526–8532.
- [27] S. Sukhov and A. Dogariu, “On the concept of tractor beams”, *Optics Letters*, 35 (2010) 22, 3847.
- [28] Jun Chen, Jack Ng, Z. Lin and C. T. Chan, “Optical pulling force”, *Nature Photonics*, 5 (2011) 531.
- [29] J. T. Costa, M. G. Silveirinha, and A. Alú, “Poynting vector negative-index metamaterials”, *Phys. Rev. B* 83 (2011) 165120.
- [30] A. Novitsky, C. W. Qiu and H. Wang, “Single Gradientless Light Beam Drags Particles as Tractor Beams”, *Phys. Rev. Lett* 107 (2011) 203601.
- [31] A. Novitsky, C.W. Qiu and A. Lavrinenko, “Material-Independent and Size-Independent Tractor Beams for Dipole Objects”, *Phys. Rev. Lett.* 109 (2012) 023902.
- [32] N. Wang, J. Chen, S. Liu and Z. Lin, “Dynamical and phase-diagram study on stable optical pulling force in Bessel beams”, *Phys. Rev. A* 87 (2013) 063812.
- [33] P. Vaveliuk, O. Martinez-Matos, “Negative propagation effect in nonparaxial Airy beams ”, *Opt. Express* 24 (2012) 24, 26913.
- [34] P. S. Tan, et al “Surface plasmon polaritons generated by optical vortex beams” , *Appl. Phys. Lett* 92 (2008) 111108.
- [35] M. Ornigotti and A. Aiello, “Surface angular momentum of light beams”, *Opt. Express* 22 (2014) 6586.
- [36] M. Duocastella and C.B. Arnold, “Bessel and annular beams for materials processing” *Laser Photonics Rev.* 6, No. 5 (2012) 607621.
- [37] C. Pfeiffer and A. Grbic, “Controlling Vector Bessel Beams with Metasurfaces”, *Phys. Rev. App.* 2 (2014) 044012.
- [38] F.G. Mitri, et al, “Optical tractor Bessel polarized beams”, *J Quant Spectrosc Radiat Transf* 187 (2017) 97.
- [39] H. Shoorian, Scattering of linearly polarized Bessel beams by dielectric spheres, *Journal of Quantitative Spectroscopy & Radiative Transfer* 199 (2017) 12.
- [40] S. Sukhov and A. Dogariu, “On the concept of tractor beams, *Opt. Lett.* 35 (2010) 3847.
- [41] O. Brzobohaty et al, “Experimental demonstration of optical transport, sorting and self-arrangement using a tractor beams, *Nature Photonics* 7 (2013) 123.
- [42] M. Mazilu, D. J. Stevenson, F. Gunn-Moore, K. Dholakia, “Light beats the spread: non-diffracting ” beams, *Laser & Photonics Reviews*, 4 (2010) 4, 529–547 .
- [43] Boyer C.P., Kalnins E.G. and W. Miller Jr., “Symmetry and separation of variables for the Helmholtz and Laplace equations,” *Nagoya Math. J.*, 60 (1976) 35–80.
- [44] D. Sarkar and N. J. Halas, “General vector basis function solution of Maxwells equations”, *Phys. Rev. E* 56 (1997) 1.
- [45] N. A. Gumerov, R. Duraiswami “A scalar potential formulation and translation theory for the time-harmonic Maxwell equations”, *J. Comp. Phys.* 225 (2007) 206–236.
- [46] J.A. Stratton , *Electromagnetic Theory*, McGraw-Hill, (1941).

- [47] K. Volke-Sepulveda and E. Ley-Koo, “General construction and connections of vector propagation invariant optical fields: TE and TM modes and polarization states,” *J. Opt. A: Pure Appl. Opt.*, 8 (2006) 10, 867-877.
- [48] S. Mishra, “A vector wave analysis of a Bessel beam,” *Opt. Comm.*, 85 (1991) 159–161.
- [49] Z. Bouchal and Z.M. Olivik, “Non-diffractive vector Bessel beams,” *J. Modern Opt.*, 42 (1995), 1555–1566.
- [50] Z. Bouchal, “Nondiffracting Optical Beams: Physical Properties, Experiments, and Applications,” *Czechoslovak Journal of Physics*, 53 (2003), 537–578.
- [51] A. Flores-Pérez, J. Hernández, R. Jáuregui and K. Volke-Sepúlveda, “Experimental generation and analysis of first-order TE and TM Bessel modes in free space,” *Opt. Letters*, 31 (2006) 11, 1732–1734.
- [52] J.D. Jackson, *Classic Electrodynamics*, Third Edition, Wiley (1999).
- [53] J. Bajér and R. Horák, “Nondiffractive fields,” *Phys. Rev. E*, 54 (1996) 3, 3052–3054.
- [54] I. Rondon-Ojeda and F. Soto-Eguibar, “Electromagnetic Field Theory for Invariant Beams Using Scalar Potentials”, *PIER B*, 66 (2016) 49-61.
- [55] C. L. Hernandez-Cedillo, S. Bernon, H. Hattermann, J. Fortgh, and R. Jauregui, “Scattering of dilute thermal atom clouds on optical Weber beams”, *Phys. Rev. A* 87 (2013) 023404.
- [56] A. Ortiz-Ambríz, J. C. Gutiérrez-Vega, and Dmitri Petrov, “Manipulation of dielectric particles with nondiffracting parabolic beams”, *J. Opt. Soc. Am. A* 31 (2014) 2759–2762.
- [57] M. A. Bandres, “Accelerating parabolic beams”, *Optics Letters*, 33, 1678 (2008).
- [58] J. A. Davis, M. J. Mitry, M. A. Bandres, and Don M. Cottrell, “Observation of accelerating parabolic beams”, *Optics Express*, 16(17) (2008) 12866–12871.
- [59] M. A. Bandres and B.M. Rodríguez-Lara, “Nondiffracting accelerating waves: Weber waves and parabolic momentum”, *New Journal of Physics*, 15 (2013) 013054.
- [60] B. M. Rodríguez-Lara, “Normalization of optical Weber waves and WeberGauss beams”, *J. Opt. Soc. Am. A* (2010) 27, 2.
- [61] A. V. Novitsky and L. M. Barkovsky “Poynting singularities in optical dynamic systems”, *Phys. Rev. A* 79 (2009) 033821.
- [62] Cheng-Wei Qiu, Darwin Palima, Andrey Novitsky, Dongliang Gao, Weiqiang Ding, Sergei V. Zhukovsky, Jesper Gluckstad, “Engineering light-matter interaction for emerging optical manipulation applications”, *Nanophotonics*. 3 (3) (2014), 181-201.